Nuclear Instruments and Methods in Physics Research A 737 (2014) 155–162

Contents lists available at ScienceDirect

Nuclear Instruments and Methods in Physics Research A

journal homepage: www.elsevier.com/locate/nima

Technical Notes

Simulating response functions and pulse shape discrimination for organic scintillation detectors with Geant4

Zachary S. Hartwig [a,*], Peter Gumplinger [b,1]

[a] Department of Nuclear Science and Engineering, MIT, Cambridge MA, USA
[b] TRIUMF, Vancouver, BC, Canada

ARTICLE INFO

Article history:
Received 16 August 2013
Received in revised form
26 October 2013
Accepted 7 November 2013
Available online 15 November 2013

Keywords:
Geant4
Scintillation detector
Detector simulation
Response functions
Pulse shape discrimination
Liquid organic scintillators

ABSTRACT

We present new capabilities of the Geant4 toolkit that enable the precision simulation of organic scintillation detectors within a comprehensive Monte Carlo code for the first time. As of version 10.0-beta, the Geant4 toolkit models the data-driven photon production from any user-defined scintillator, photon transportation through arbitrarily complex detector geometries, and time-resolved photon detection at the light readout device. By fully specifying the optical properties and geometrical configuration of the detector, the user can simulate response functions, photon transit times, and pulse shape discrimination. These capabilities enable detector simulation within a larger experimental environment as well as computationally evaluating novel scintillators, detector geometry, and light readout configurations. We demonstrate agreement of Geant4 with the NRESP7 code and with experiments for the spectroscopy of neutrons and gammas in the ranges 0–20 MeV and 0.511–1.274 MeV, respectively, using EJ301-based organic scintillation detectors. We also show agreement between Geant4 and experimental modeling of the particle-dependent detector pulses that enable simulated pulse shape discrimination.

1. Introduction

The simulation of organic scintillation detectors in neutron and gamma fields has long been of interest to the detector physics community for two primary reasons. First, simulation helps interpret the complex detector response functions that are generated by the nonlinear production of scintillation photons as a function of energy deposited and ionizing particle type. Second, simulation can easily generate a large number of detector response functions for various incident particles, which can be difficult to obtain experimentally. These response functions are required as inputs to unfolding codes that deconvolve the incident particle energy spectrum from the detector response. In addition, simulation can play an important role in the computational design and optimization of new types of particle detectors that are based on organic scintillators.

In this paper, we present the implementation and validation of new organic scintillation detector modeling capabilities contained in the Geant4 toolkit as of version 10.0-beta. The method enables the user to fully simulate time-resolved production (linear or nonlinear), transport, and readout of photons in a detector of arbitrary geometry, scintillator choice, structural materials, and light readout configuration, all potentially within the complexity of an encompassing experiment geometry. This is the first time that such comprehensive detector modeling can be performed within a single Monte Carlo (MC) code, leading to significant improvements in the simulation of detector response in complex environments and the optimization of advanced design for scintillation detectors.

This paper is structured as follows: Section 2 describes the motivation behind this work; Section 3 overviews the simulation capabilities of Geant4 for organic scintillators; Section 4 describes the hardware used to experimentally validate Geant4 for organic scintillation detectors; Section 5 demonstrates Geant4's ability to correctly simulate organic scintillation detector response functions for incident neutrons (0–20 MeV) and gammas (0.511–1.274 MeV); and Section 6 demonstrates Geant4's ability to correctly simulate the timing properties of individual scintillator light pulses, which enables the simulation of pulse shape discrimination.

2. Motivation

The most widely used configuration for organic scintillation detectors is a right cylinder scintillator coupled to a photomultiplier tube (PMT) of similar size to optimize light collection. However, new scintillator materials, such as pulse shape discriminating plastic [1] and new light readout devices, such as silicon photomultipliers

* Corresponding author. Tel.: +1 617 253 0025.
E-mail address: hartwig@psfc.mit.edu (Z.S. Hartwig).
[1] Member of the Geant4 Collaboration.

0168-9002/$ - see front matter © 2013 Elsevier B.V. All rights reserved.
http://dx.doi.org/10.1016/j.nima.2013.11.027

(SiPMs), can now be used to fabricate detectors in a wide variety of complex geometries, materials, and light readout configurations. For these "advanced" organic scintillation detectors, the capability to perform high fidelity modeling of the detector response functions and pulse shape discrimination (PSD) would greatly enhance computational detector design.

Existing codes are not well suited to such work. Although used successfully for decades to model organic scintillation detectors, previous codes such as SCINFUL [2] and NRESP7 [3] are limited to right cylinder geometries, provide limited particle sources, do not model the light readout device, and restrict the simulation boundary to the detector itself. Recently, codes such as MCNP-PoliMi [4] and MCNPX-PHOTRACK [5] have extended somewhat the detector complexity and simulation domain that can be modeled but require significant post processing and code coupling. Although MCNPX-PHOTRACK can estimate the effect of optical parameters on PSD, neither code can directly simulate PSD via the time-resolved production, transport, and detection of optical photons.

One of the principal motivations for this work was to develop a single MC code that could comprehensively model the optical physics of advanced organic scintillation detectors. This can play an important role in guiding detector design and optimization. A second motivation was the desire to include this capability within the framework of a general purpose MC code – Geant4 in particular – in order to calculate detector response functions within a larger simulated experiment. This is crucial for a Geant4-based simulation of a new type of particle accelerator-based instrument, which studies the evolution of materials inside magnetic confinement fusion reactors [6].

3. Geant4

Geant4 is an object-oriented C++ Monte Carlo toolkit for simulating the passage of particles through matter [7]. Most aspects of simulating EJ301-based scintillation detectors with Geant4 have been extensively studied [8–12].

All of these studies, however, neglect the production, transportation, and detection of scintillation photons, choosing to score the energy deposition in the scintillator volume and then apply scintillation response and detector resolution functions to replicate the full experimental detector response. While successful in many applications, this approach is not ideal as it obscures the influence of optical properties on the detector response, requires substantial knowledge of the scintillator light response and detector energy resolution, necessitates post-processing work by the user to generate detector response functions, and is not applicable to computationally exploring complex detector geometries or nonstandard light readouts.

As of Geant4.10.0-beta (released June 2013), a new model for energy- and particle-dependent scintillation, coupled to the pre-existing optical physics capabilities, enables the user to simulate an organic scintillation detector of arbitrary complexity with a minimum amount of overhead. We briefly describe the new scintillation model and optical transport capabilities of Geant4 below; for detailed description and instruction on implementing these features in user simulations, the reader is referred to Section 5.2.5 of the Geant4 User's Guide for Application Developers [13].

3.1. Scintillation model

In Geant4, as in all other MC codes, a continuous particle trajectory is necessarily broken into many small steps in order to correctly simulate the passage of the particle through matter, which has important implications for simulating the scintillation light response. In scintillators with a linear response, light production is directly proportional to the ionizing energy deposited in the scintillator. Thus, the total light produced along a particle track in the scintillator can be computed as the sum of the light produced in smaller steps without regard for the kinetic energy of the ionizing particle at each energy-depositing step.

In scintillators with a nonlinear response, the light produced in each step must be computed as

$$L_{\text{step}} = L(T, x) - L(T - E_{\text{dep}}, x) \tag{1}$$

where L is the number of scintillation photons, T is the kinetic energy of the charged particle before the step, E_{dep} is the total ionizing energy deposited in the scintillator during the step, and x is the charged particle type depositing energy. In addition to correctly modeling the total light produced by a multiple step ionizing particle track in a scintillator, this methodology accounts for two important cases. First, light is produced correctly for incomplete energy deposition of the charged particle, such as is the case where the particle exits the scintillator volume ("wall effects") or in the case that the particle is absorbed in a nuclear reaction. Second, the scintillation photon density is larger in the high-kinetic energy portion of the ionizing particle track in the usual case where the nonlinear photon yield increases with particle energy.

3.2. Optical physics models

In Geant4, optical photons are linearly transported in media with an imputed index of refraction, until they are either bulk absorbed, are Mie or Rayleigh scattered, or encounter a medium boundary. The boundary can be between two dielectric materials or a dielectric and a metal. In the latter case, the photons can be reflected or absorbed, in which case absorbed photons can be deemed detected after sampling a user-specified wavelength dependent detection efficiency.

The UNIFIED model [14], originally developed for the DETECT MC program [15] provides a range of different reflection mechanisms (specular lobe, specular spike, Lambertian and back-scatter spike) and polished and rough optical surfaces. A simpler roughness model, GLISUR [16], carried over from an earlier version of Geant(3) is also available. For an entirely empirical surface model, the results of measurements of the angular reflectivity distribution inside of a BGO crystal, for combinations of common surface treatments and different applied reflectors, are available in look-up-tables (LUTs) [17].

A scintillator material is characterized by its photon emission spectrum, its rise time, and its exponential decay time components. Two time decay components are possible with defined relative strength, and they can have different emission spectra. A characteristic light yield is part of the scintillator's material definition, with the actual simulated number statistically sampled around this mean. When the scintillation yield is a non-linear function of the energy deposited and varies between particle types, an array of total scintillation light yields as a function of deposited energy may be defined for protons, electrons, deuterons, tritons, alphas, and carbon ions, enabling precision modeling of any scintillator's light response.

4. Experimental setup

This sections describes the hardware setup – particle detectors and data acquisition system – used to experimentally validate the capability of Geant4 to simulate organic scintillation detectors.

4.1. Particle detectors

The organic scintillator material used in the detectors was the xylene- and napthalene-based organic liquid known variably by its manufacturer's product code: EJ301 (Eljen Technology), BC501A (Saint-Gobain), or NE213 (Nuclear Enterprises). The essential properties of this scintillator are described in Table 1. The properties of EJ301 have been extensively reported in the literature, such as material properties [18], optical properties [19–21], interaction mechanisms with fast neutrons and gammas [22], and performance as a detector for neutrons and gammas [22,23]. In addition, a number of EJ301 light responses to various particle and energy ranges have also been published [24–27,10].

For the purpose of demonstrating the flexibility of organic scintillation detector simulation with Geant4, two different EJ301-based detectors, shown together in Fig. 1, were used in this work. The first is a large rectangular scintillation detector custom-manufactured by Scionix (Detector #1). The rectangular cavity that houses the EJ301 liquid organic scintillator measures $25.0 \times 25.0 \times 8.2$ cm and is surrounded by an approximately 2.0 cm thick aluminum case for structural support; a single 3-in. PMT, perpendicularly attached to the short dimension of the detector, provides light readout. While the large detector dimensions provide excellent detection efficiency, the single PMT readout results in long light collection times as the light must bounce around the scintillation cavity before reaching the PMT photocathode. The result is a degraded time response of the scintillation pulse and poor pulse shape discrimination at lower incident particle energies.

The second detector is a small cylindrical detector assembled in-house (Detector #2). A $2.5\phi \times 2.7$ cm right cylinder of EJ301 liquid organic scintillator is coupled directly to a 1-in. Hamamatsu R6095 PMT with a bialkali photocathode. The scintillator cavity is covered with a diffuse titanium dioxide reflector paint, and the scintillator light passes through a 6 mm borofloat glass window before reaching the PMT. Although the small detector size results in low absolute detection efficiency, the exact geometrical match between the scintillator cavity, borofloat window, and PMT photocathode results in fast light collection times and excellent pulse shape discrimination.

Table 1
Basic properties of EJ301 liquid organic scintillator [18].

Quantity	Value
Mass density (g/cm^3)	0.874
Atomic C:H ratio	1.212
Refractive index	1.505
Light/MeV (photons)	~12 000
Peak emission wavelength (nm)	425
Light decay components (ns)	3.0, 32, 270

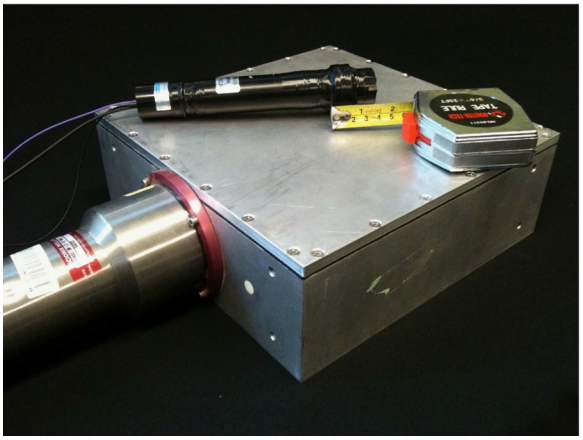

Fig. 1. The scintillation detectors used in this paper. The large, rectangular detector on the bottom is a custom $25.0 \times 25.0 \times 8.2$ cm EJ301 liquid scintillator with a single 3-in. PMT and was manufactured by Scionix. The small, cylindrical detector on top is a 2.5×2.7 cm EJ301 liquid scintillator with a single 1-inch PMT and was assembled in house. Approximately 7 cm of measuring tape is shown for scale.

4.2. Data acquisition

Digital acquisition and pulse processing were used to handle the detector readout and analysis for all experiments in this paper. The data acquisition system was composed of electronics from CAEN S.p.A:

- V1720 digitizer (8 channel, 250 MS/s, 12-bit)
- V6534 HV supply (6 channel, 6 kV, 1 mA)
- V1718 USB-VME interface board
- VME8004B powered enclosure

A PC connects to the VME system via USB and runs custom data acquisition software based on the ROOT toolkit [28]. The software provides control of all the VME boards and a digital oscilloscope, digital multichannel analyzer, and persistent digitized pulse storage on the hard disk drive. For these experiments, all detector pulses were digitized and stored in compressed ROOT files for offline analysis with a custom ROOT-based data analysis tool that provides all the features of a modern digital spectroscopy system.

5. Validating simulated EJ301 detector responses

In order to confirm the capability of Geant4 to correctly simulate the detector responses of organic scintillators, we performed a series of computational and experimental validation tests. The tests attempted to validate the response functions generated by Geant4 against a leading organic scintillation detector simulation code and our own experiments. The tests covered a wide energy range for both gammas (0.511–1.274 MeV) and neutrons (0–20 MeV). All Geant4 detector response functions were produced with version 10.0-beta, using the EJ301 light responses of Verbinski [24] to model the scintillation light output as functions of energy deposited and particle type.

The Geant4 physics list was constructed using the standard prepackaged and validated class collections of relevant physics: `G4EmStandardPhysics` for electromagnetic interactions; `HadronPhysicsQGSP_BIC_HP` and `HadronElasticPhysicsHP` for hadronic interactions; `G4DecayPhysics` for particle decay; and `G4OpticalPhysics` to include the production and transportation of scintillation photons. The neutron high precision (HP) data transport model used the standard G4NDL4.3 neutron data library that is distributed with Geant4.

5.1. Ensuring equivalent detector response functions

When comparing two organic scintillation detector response functions, the response functions must have identical units and be appropriately scaled to one another by requiring that integrals under the two response functions for identical ranges are equal.

In Geant4, response functions are generated by histogramming the number of detected photons per event for all simulated events, giving the X-axis units in detected photons by default. The detector response produced by many other simulation codes is typically given as light versus counts, where light is in the ubiquitous units of MeV-electron-equivalent, or MeVee. In this paper, the unit MeVee is defined as the scintillation light produced by 1 MeV deposited in

the scintillator by electrons. In order to compare other codes to Geant4, the light value can be multiplied by the scintillator photon yield – 12 000 photons per MeV deposited by electrons for EJ301 – to convert the *X*-axis units of the response function histogram from MeVee to total detected photons.

Comparing Geant4 to experimental response functions is more complicated due to detector calibration. Typically, two or more monoenergetic gamma energies are used to experimentally place the *X*-axis calibration on an absolute linear scale [24], which determines the conversion from pulse height (units defined by the data acquisition system) to light produced (units of MeVee). Because the approach taken by Geant4 simulates physical reality to such a high degree, a simulated calibration – identical to the experimental one – must be performed to convert the *X*-axis of the simulated response function histogram from detected photons to MeVee. Once the calibration is established – experimental and simulated – Geant4 and experimental response functions for any equivalent particle flux may be correctly compared.

5.2. Computational validation against NRESP7

NRESP7 is one of the most widely used and validated codes for the simulation of EJ301-PMT detectors for incident fast neutrons up to 20 MeV [3]. It has been successfully used at Physikalisch-Technische Bundesanstalt in Germany for almost 30 years for the simulation of EJ301-based detector response functions [29].

A simulated 5.08$\phi \times$ 5.08 cm right cylinder of EJ301 was constructed in Geant4 and NRESP7. We ensured that the detector geometry and optical properties were identical between the two codes. The detectors were then irradiated with monoenergetic neutrons along the axial dimension of the scintillator up to 19.9 MeV, the high energy cutoff for NRESP7 and Geant4's NeutronHP model.

Six results comparing detector response functions from NRESP7 and Geant4 at different incident neutron energies are shown in Fig. 2; the shaded area depicts the integration range used to scale the Geant4 response functions to those of NRESP7. Overall, the comparison shows close agreement between the two codes over the entire detector response functions and across the energy range of incident neutrons. Several features in particular demonstrate excellent agreement: the position of the high energy edge, defined by the maximum energy transfer in the elastic scattering ^{1}H(n,n)^{1}H reaction; the peaked hump just below the high energy edge caused by multiple scattering in a single event within the scintillator volume; and the rise at low energies for incident neutrons below 12 MeV, defined by the increase in light contribution from nuclear reaction exit channels which include alphas and ions.

There are two slight differences, one expected and one unexpected. The expected difference occurs in the disagreement of the low light region of the detector response function for incident neutron energies above approximately 12 MeV. The cause is the inability of the NeutronHP model in Geant4 to correctly handle breakup reactions that become important at high neutron energies. Reactions such as

$$^{12}\mathrm{C}(\mathrm{n},\mathrm{n}')^{12}\mathrm{C}^{*} \Rightarrow 3\alpha, \tag{2}$$

lead to light contributions in the low light region of the detector response function due to energy deposition by deuterons, alphas, and heavier ions, which produce significantly less light than electrons or protons for the same energy deposited. NRESP7 correctly includes these reactions, which lead to the higher light response. This discrepancy has been reported in the literature [10].

While the breakup reactions exist in the G4NDL4.3 neutron data library, the `G4NeutronHP` transport model presently handles the reaction as one-step inelastic reactions and does not model the breakup of the excited nuclei. For the example reaction presented in Eq. (2), the ^{12}C* does not decay into three alpha particles, leading to an underpredication of light in the low light region of the detector response function. An update to `G4NeutronHP`, which would enable the correct handling of breakup reactions, is presently under development and is expected in a future Geant4 release.

The second, unexpected discrepancy in the comparison to NRESP7 occurs in the slight underprediction by Geant4 for the lower light portion of the scattering continuum for incident neutrons below 5 MeV. This effect might be explained by either slight disagreements in the ^{1}H(n,n)^{1}H differential cross-section or in differences of light transport between Geant4 and NRESP7.

While the latter issue warrants further study, we believe that overall the results show excellent agreement between the two codes. More importantly, the NRESP7 results shown in Fig. 2 have been shown to replicate experimental measurements with high accuracy [29], giving further validity to Geant4's ability to correctly simulation the detector response functions to neutrons for EJ301.

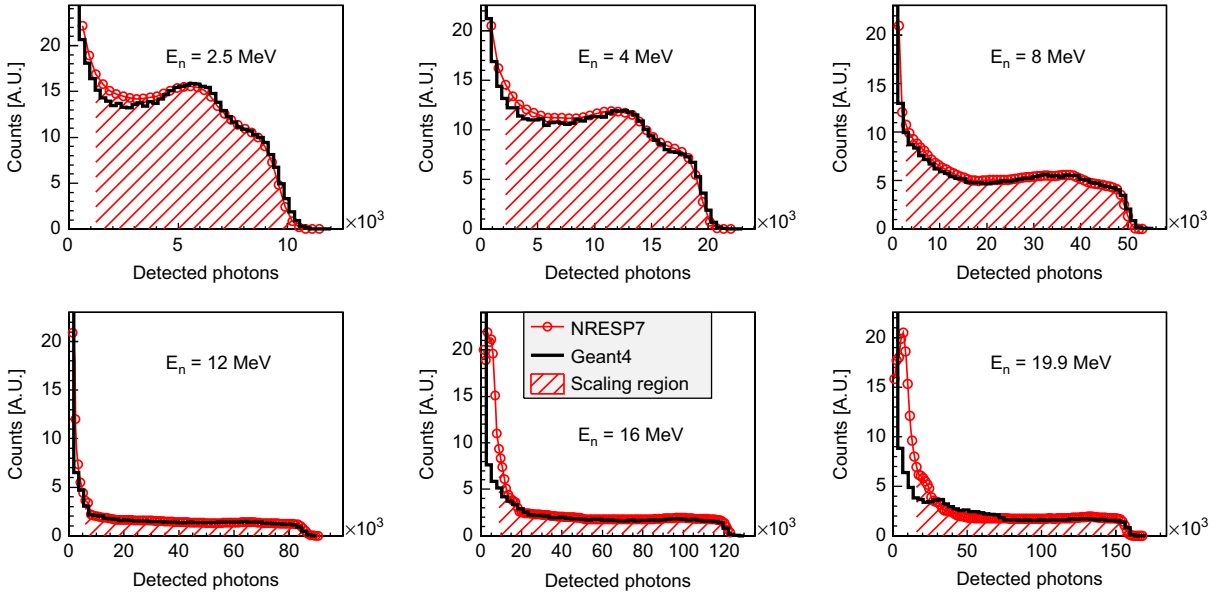

Fig. 2. Comparisons between NRESP7 and Geant4 simulated detector responses of a 5.08$\phi \times$ 5.08 cm right cylinder of EJ301 to monoenergetic neutrons.

5.3. Experimental validation against ^{241}AmBe neutrons

For this experiment, Detector #1 ($25.0 \times 25.0 \times 8.2$ cm cell of EJ301) was exposed to an ^{241}Americium-Beryllium source (^{241}AmBe) with the goal of replicating the experimental neutron detector response with Geant4. The source was placed approximately 15 cm above the center of the square face of the detector. Two sets of data were taken, one with the source in place and one with the source removed. The latter spectrum was subtracted from the former to remove the particle background from cosmic rays and terrestrial decay events. Data was collected long enough to obtain a smooth experimental detector response function with excellent statistics. For the Geant4 simulation, the complex ^{241}AmBe neutron emission spectrum was taken from the recommended ISO standard [30], and gammas, produced by inelastic neutron collisions with the detector, were filtered out of the final detector response function.

Because the detector is used in a mixed neutron and gamma field, pulse shape discrimination of the experimental detector waveforms must be performed to ensure only waveforms generated by neutron interactions are included in the detector response. The experimental PSD for Detector #1 using the ^{241}AmBe source is shown in Fig. 3. In this case, the PSD was computed by histogramming the digital integral of the tail pulse and the integral of the total pulse in two dimensions. The tail pulse is defined as the region of the pulse between approximately 30 ns and 150 ns after the start of the pulse, where the charge differential between electron- and proton-induced pulses is strongly evident. The units of the integrals are given in analog-to-digital conversion (ADC) units, which are simply the discrete values assigned to the analog detector voltage pulse in our data acquisition system.

While excellent PSD is achieved over the majority of the energy of incident particles, the relatively large size of Detector #1 coupled to the single 3-in. PMT readout leads to relatively poor PSD at the lowest energies. To determine the lowest energy at which particles can be discriminated, Gaussians are fitted to the neutron and gamma distributions that appear in a 1D projection of the 2D PSD histogram as shown in Fig. 4. The PSD figure of merit (FOM) is then defined as

$$\mathrm{FOM}(L) = \frac{\Delta}{\Gamma_\gamma + \Gamma_n}, \tag{3}$$

where L is the light produced in the scintillator, Δ is the separation between Gaussian fit means, and Γ is the full-width-half-maximum of the Gaussian fits to the gamma (γ) and neutron (n) contributions [31]. An FOM greater than unity confirms that the neutron and gamma distributions have essentially zero overlap and provides confidence in PSD at this light level. For Detector #1, the FOM at 0.5 MeVee is 1.03, which we consider to be the lowest light levels at which PSD is adequate for separating neutron and gamma events.

The experimental neutron detector response function for the ^{241}AmBe source is compared to the simulated Geant4 response function in Fig. 5. The simulated response is scaled to match the experimental response by equilibrating integrals of the response functions from 1.3 to 6.3 MeVee. Close agreement between the experimental and simulated response functions are achieved over almost the entire response within the statistical uncertainties; a few spurious high energy events appear in the simulated spectrum. The slight deviation at lower energies in the experimental spectrum is attributed to deteriorating PSD enabling leakage of gamma events into the neutron spectrum; the experimental spectrum is cutoff at the PSD-determined lower threshold of 0.5 MeVee. Overall, the results indicate that Geant4 is capable of correctly simulating organic scintillation detector response functions for incident neutrons in the 0–10 MeV range, despite an unusually large suboptimal detector and complicated incident neutron spectrum.

5.4. Experimental validation against monoenergetic gammas

For this experiment, Detector #2 ($2.5\phi \times 2.7$ cm right cylinder of EJ301) was exposed to three monoenergetic gammas from standard radioisotope source: 0.662 MeV gammas from ^{137}Cs in

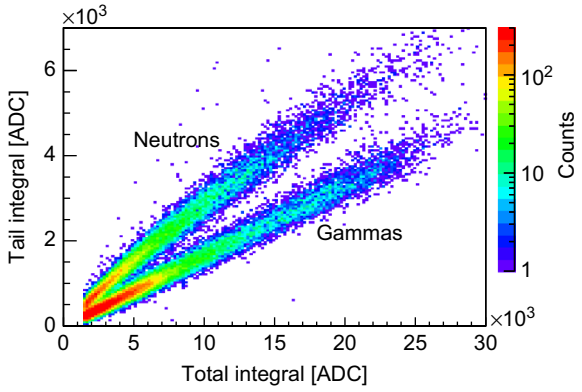

Fig. 3. The result of digital pulse shape discrimination (PSD) using the charge comparison method for Detector #1 when exposed to the ^{241}AmBe source. The large size of the scintillator volume ($25.0 \times 25.0 \times 8.2$ cm) and only a single 3-in. PMT of the detector result in degraded PSD at lower energies due to poor light collection. ADC units are the digital value assigned by the waveform digitizer to the incident analog detector voltage pulse. For reference: 0.5 MeVee corresponds to approximately 2750 ADC on the X-axis.

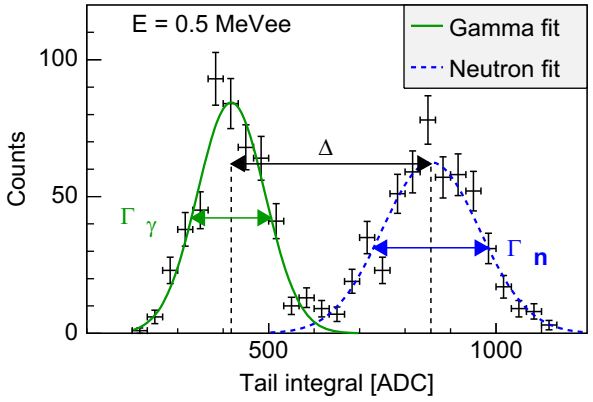

Fig. 4. Evaluating the PSD figure of merit (FOM) for Detector #1 using the ^{241}AmBe source. The FOM, defined in Eq. (3), is 1.03 at 0.5 MeVee, which we define as the lower threshold for performing acceptable PSD in this detector.

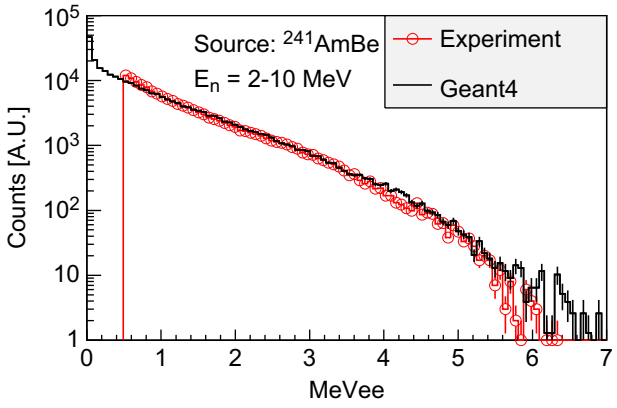

Fig. 5. Comparison between experimental and simulated detector responses for Detector #1 when exposed to the ^{241}AmBe source.

the first run; and 0.511 and 1.274 MeV gammas simultaneously from ^{22}Na in the second run. The sources were placed approximately 5 cm from the flat face of the cylindrical scintillator housing and were aligned with the cylinder's axis of symmetry. Data was collected long enough to obtain a smooth experimental response function with excellent statistics. Because essentially zero neutrons interacted with detector during the few seconds of source irradiation, PSD was not required. A lower light threshold of 0.15 MeVee was applied to the experimental data to prevent unphysical results created by noise and extrapolation well below the calibration data points.

The experimental detector response function for 0.662 MeV gammas compared to the simulated response function in Fig. 6. The simulated and experimental detector responses are closely matched showing agreement to better than a few percent over most of the light range. Geant4 simulation correctly replicates the position of the Compton edge, the shape of the broad Compton continuum, and the intrinsic detector resolution. Compared to experiment, simulation results in a more sharply defined peak at 0.43 MeVee and slightly underpredicts the counts at the lowest light levels. We attribute the latter issue to a small number of downscattered gammas from the PMT and ambient geometry in the experiment that were not modeled in the simulation.

Similarly, the experimental detector response function for the simultaneous exposure to 0.511 and 1.274 MeV gammas, shown in Fig. 7, agrees to within a few a percent over the majority of the light range. The expected spectral features in the experimental response function are closely reproduced by the Geant4 simulation, including the ratio of 0.511–1.274 gammas, indicating that the absolute detector efficiency is correctly simulated as well. The main disagreement is in the slightly more peaked distribution around 0.3 MeVee.

These results indicate that Geant4 can simulate EJ301 detector responses to gammas in the 0.511–1.274 MeV gamma energy range to better than 5% agreement over most of the response function. While the simulated response showed slightly sharper peaks than the experimental response – perhaps indicative of slight differences in light transport between the simulation and experiment – Geant4 can reproduce with high accuracy many of the important spectral features such as the shape and location of the smeared Compton edges and the shape of the Compton scattering continuum.

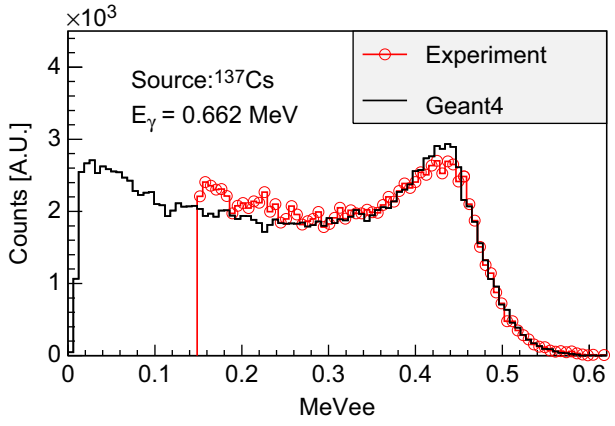

Fig. 6. Comparison between experimental and Geant4 simulated detector responses for Detector #2 when exposed to 0.662 MeV gammas from ^{137}Cs.

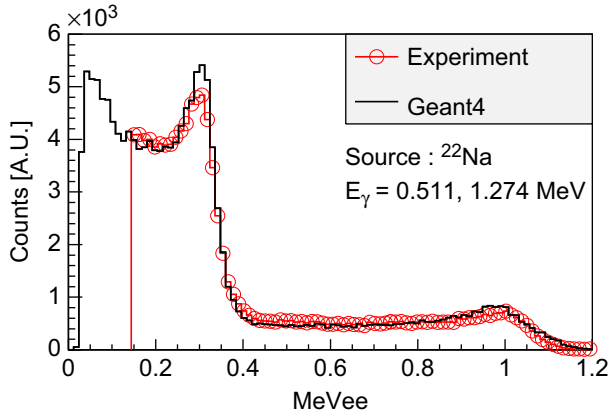

Fig. 7. Comparison between experimental and Geant4 simulated detector responses for Detector #2 when exposed to 0.511 and 1.274 MeV gammas from ^{22}Na.

6. Validating simulated time responses

To validate the capability of Geant4 to study the timing properties of organic scintillators, Geant4 was used to simulate individual pulses of scintillation light from EJ301 in response to different incident particles. Proton pulses can be obtained through neutron elastic scattering off hydrogen in the scintillator while electron pulses can be obtained from the Compton scattering of gammas off atomic electrons. The digitized experimental pulses were obtained from the same data set acquired with the ^{241}AmBe source that was discussed in Section 5 since that source provides neutrons and gammas simultaneously. Comparisons of simulated proton and electron pulses to the corresponding experimental pulses are shown in Fig. 8. To produce an equivalent comparison, the pulse peak positions were used to align the pulses on the time axis, and the experimental pulse was scaled to match the peak amplitude of the simulated pulse. While Geant4 does not accurately capture the pulse rise time, the crucial components of the pulse for distinguishing particles – the decay tail – is replicated to high degree.

Two conclusions can be drawn. First, Geant4 models the first two light decay components very well for both electrons and

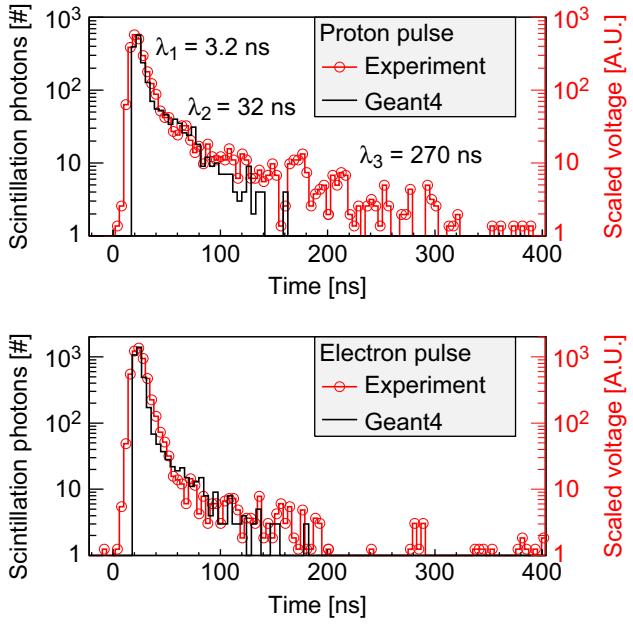

Fig. 8. Comparisons between experimental and simulated individual detector pulses produced by a ~1 MeV proton (top) and a ~1 MeV electron (bottom) in Detector #2. The larger light fraction in the slow decay component for protons compared to electrons is clearly visible and forms the basis for pulse shape discrimination. Geant4 is presently only capable of simulating the first two decay components.

protons, correctly replicating the experimental pulse width and shape. This confirms that Geant4 correctly handles the time-dependent production, transport, and detection of scintillation photons relative to the arrival of the energy-depositing particle in the detector. Second, Geant4 is capable of simulating the energy distributed between the first and second light decay components for different particles, as evident by the larger second-component decay tail for the proton pulses.

Because the simulated pulses reflect the features that form the basis of distinguishing particle types using the decay tail shape, Geant4 is capable of simulating PSD, which was performed for Detector #2 in response to neutrons and gammas from the ^{241}AmBe source. The results appear in Fig. 9 and reflect the excellent PSD capability enabled by the efficient light collection of the small, optimized Detector #2. More importantly, because scintillation photons are generated, transported, and detected using the full MC features described in this paper, synthetic PSD can be performed for a detector of arbitrary geometrical complexity and light readout configuration. This enables the detector physicist to evaluate computationally, for example, the effect on PSD capability of scintillator size and geometry, long light guides or fibers, the substitution of large PMTs with small SiPMs, or various reflective coatings.

7. Conclusion

We have presented new features of the Geant4 toolkit that enable users to correctly model the detector responses and time-dependent pulses of organic scintillation detectors in response to neutrons and gammas. We have demonstrated the excellent agreement of Geant4 with one of the leading detector simulation codes, NRESP7, and with our own experiments for neutrons and gammas in the energy range of 0–20 MeV and 0.511–1.274 MeV, respectively. We have shown that Geant4 correctly simulates the time-resolved generation, transport, and detection of scintillation photons, as well as presented an example of simulating pulse shape discrimination in EJ301-based detectors.

The features presented here provide, for the first time, the ability to simulate a detector of arbitrary complexity and configuration within a single Monte Carlo code, which has two important implications. First, with its extensive physics, geometry, and particle transport modeling, Geant4 facilitates comprehensive detector simulation within an experimental environment, a crucial need in many types of experiments. Second, new types of scintillation detectors, which deviate from the standard PMT-coupled right cylinder of liquid organic scintillator, can be modeled, from scintillator type to optical transport to light readout devices. Although we used PMT-coupled EJ301 detectors for our validation work, the extensibility of the method provides a framework for the evaluation of any type of scintillator and optical readout device so long as the scintillation response and optical property data are correctly input into Geant4.

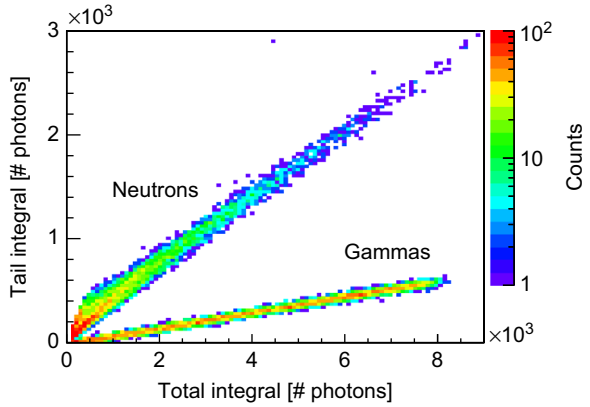

Fig. 9. An example of simulated PSD for Detector #2 when using a simulated ^{241}AmBe source. The excellent light collection of Detector #2 is evident in the clear separation of neutrons and gammas down to the lowest energies.

While previous codes will continue to serve the detector physics community well for certain applications, Geant4 now provides a more flexible and extensible environment for the simulation of organic scintillation detectors. This capability should significantly aid users who require a more powerful capability to simulate detectors within larger experiments or to computationally evaluate advanced detector designs.

Acknowledgments

The authors are grateful to Andreas Zimbal (PTB, Germany) for sharing the NRESP7 neutron response code and to Chuck Hurlbut (Eljen Technology, USA) for technical discussion of liquid organic scintillators. The authors are also grateful to the Geant4 Publications Board for their careful review of and constructive suggestions for the manuscript. This work was supported in part by U.S DOE Grant DE-FG02-94ER54235 and Cooperative Agreement DE-FC02-99ER54512.

References

[1] N. Zaitseva, B.L. Rupert, I. Paweczak, A. Glenn, H.P. Martinez, L. Carman, M. Faust, N. Cherepy, S. Payne, Nucl. Instrum. Methods Phys. Res. Sect. A Acceler. Spectrometers Detectors Assoc. Equip. 668 (2012) 88.
[2] J. Dickens, A Monte Carlo Based Computer Program to Determine a Scintillator Full Energy Response to Neutron Detection for En Between 0.1 and 80 MeV, ORNL-6463, 1988.
[3] G. Dietze, H. Klein, NRESP4 and NEFF4 : Monte Carlo codes for the calculation of neutron response functions and detection efficiencies for NE213 scintillation detectors, PTB Report PTB-ND-22, 1982.
[4] S.A. Pozzi, M. Flaska, A. Enqvist, I. Pzsit, Nucl. Instrum. Methods Phys. Res. Sect. A Acceler. Spectrometers Detectors Assoc. Equip. 582 (2007) 629.
[5] M. Tajik, N. Ghal-Eh, G. Etaati, H. Afarideh, Nucl. Instrum. Methods Phys. Res. Sect. A Acceler. Spectrometers Detectors Assoc. Equip. 704 (2013) 104.
[6] Z.S. Hartwig, D.G. Whyte, Rev. Sci. Instrum. 81 (2010) 10E106.
[7] S. Agostinelli, J. Allison, K. Amako, J. Apostolakis, H. Araujo, P. Arce, M. Asai, D. Axen, S. Banerjee, G. Barrand, F. Behner, L. Bellagamba, J. Boudreau, L. Broglia, A. Brunengo, H. Burkhardt, S. Chauvie, J. Chuma, R. Chytracek, G. Cooperman, G. Cosmo, P. Degtyarenko, A. Dell'Acqua, G. Depaola, D. Dietrich, R. Enami, A. Feliciello, C. Ferguson, H. Fesefeldt, G. Folger, F. Foppiano, A. Forti, S. Garelli, S. Giani, R. Giannitrapani, D. Gibin, J.J. G. Cadenas, I. Gonzlez, G.G. Abril, G. Greeniaus, W. Greiner, V. Grichine, A. Grossheim, S. Guatelli, P. Gumplinger, R. Hamatsu, K. Hashimoto, H. Hasui, A. Heikkinen, A. Howard, V. Ivanchenko, A. Johnson, F.W. Jones, J. Kallenbach, N. Kanaya, M. Kawabata, Y. Kawabata, M. Kawaguti, S. Kelner, P. Kent, A. Kimura, T. Kodama, R. Kokoulin, M. Kossov, H. Kurashige, E. Lamanna, T. Lampn, V. Lara, V. Lefebure, F. Lei, M. Liendl, W. Lockman, F. Longo, S. Magni, M. Maire, E. Medernach, K. Minamimoto, P.M. de Freitas, Y. Morita, K. Murakami, M. Nagamatu, R. Nartallo, P. Nieminen, T. Nishimura, K. Ohtsubo, M. Okamura, S. O'Neale, Y. Oohata, K. Paech, J. Perl, A. Pfeiffer, M.G. Pia, F. Ranjard, A. Rybin, S. Sadilov, E.D. Salvo, G. Santin, T. Sasaki, N. Savvas, Y. Sawada, S. Scherer, S. Sei, V. Sirotenko, D. Smith, N. Starkov, H. Stoecker, J. Sulkimo, M. Takahata, S. Tanaka, E. Tcherniaev, E.S. Tehrani, M. Tropeano, P. Truscott, H. Uno, L. Urban, P. Urban, M. Verderi, A. Walkden, W. Wander, H. Weber, J.P. Wellisch, T. Wenaus, D.C. Williams, D. Wright, T. Yamada, H. Yoshida, D. Zschiesche, Nucl. Instrum. Methods Phys. Res. Sect. A Acceler. Spectrometers Detectors Assoc. Equip. 506 (2003) 250.
[8] N. Patronis, M. Kokkoris, D. Giantsoudi, G. Perdikakis, C. Papadopoulos, R. Vlastou, Nucl. Instrum. Methods Phys. Res. Sect. A Acceler. Spectrometers Detectors Assoc. Equip. 578 (2007) 351.
[9] K. Banerjee, T. Ghosh, S. Kundu, T. Rana, C. Bhattacharya, J. Meena, G. Mukherjee, P. Mali, D. Gupta, S. Mukhopadhyay, D. Pandit, S. Banerjee, S. Bhattacharya, T. Bandyopadhyay, S. Chatterjee, Nucl. Instrum. Methods Phys. Res. Sect. A Acceler. Spectrometers Detectors Assoc. Equip. 608 (2009) 440.
[10] M. Gohil, K. Banerjee, S. Bhattacharya, C. Bhattacharya, S. Kundu, T. Rana, G. Mukherjee, J. Meena, R. Pandey, H. Pai, T. Ghosh, A. Dey, S. Mukhopadhyay, D. Pandit, S. Pal, S. Banerjee, T. Bandhop, Nucl. Instrum. Methods Phys. Res. Sect. A Acceler. Spectrometers Detectors Assoc. Equip. 664 (2012) 304.
[11] X. Xufei, Z. Xing, Y. Xi, F. Tieshuan, C. Jinxiang, L. Xiangqing, Nucl. Instrum. Methods Phys. Res. Sect. A Acceler. Spectrometers Detectors Assoc. Equip. 721 (2013) 10.
[12] S. Naeem, S. Clarke, S. Pozzi, Nucl. Instrum. Methods Phys. Res. Sect. A Acceler. Spectrometers Detectors Assoc. Equip. 714 (2013) 98.

[13] Geant4 Collaboration, Geant4 User's Guide for Application Developers, 2012.
[14] A. Levin, C. Moisan, A more physical approach to model the surface treatment of scintillation counts and its implementation into detect, TRIUMF Preprint TRI-PP-96-94, 1996.
[15] G. Knoll, T. Knoll, T. Henderson, IEEE Trans. Nucl. Sci. NS-35 (1988) 872.
[16] CERN Computing and Networks Division, Geant detector description and simulation tool, CERN PHYS260-6 tp 260-7, 1993.
[17] M. Janecek, W.W. Moses, IEEE Trans. Nucl. Sci. NS-57 (2010) 964.
[18] Eljen Technology Inc., EJ-301 Liquid Scintillator Data Sheet, 2013.
[19] F.T. Kuchnir, F.J. Lynch, IEEE Trans. Nucl. Sci. NS-15 (1968) 107.
[20] V. Filchenkov, A. Konin, V. Zinov, Nucl. Instrum. Methods Phys. Res. Sect. A Acceler. Spectrometers Detectors Assoc. Equip. 245 (1986) 490.
[21] G. Ranucci, A. Goretti, P. Lombardi, Nucl. Instrum. Methods Phys. Res. Sect. A Acceler. Spectrometers Detectors Assoc. Equip. 412 (1998) 374.
[22] G.F. Knoll, Radiation Detection and Measurement, Wiley, 2000.
[23] H. Klein, S. Neumann, Nucl. Instrum. Methods Phys. Res. Sect. A Acceler. Spectrometers Detectors Assoc. Equip. 476 (2002) 132. (International Workshop on Neutron Field Spectrometry in Science, Technology and Radiation Protection).
[24] V. Verbinski, W. Burrus, T. Love, W. Zobel, N. Hill, R. Textor, Nucl. Instrum. Methods 65 (1968) 8.
[25] R. Cecil, B. Anderson, R. Madey, Nucl. Instrum. Methods 161 (1979) 439.
[26] A. Aksoy, A. Coban, A. Naqvi, F. Khiari, J. Hanly, C. Howell, W. Tornow, P. Felsher, M. Al-Ohali, R. Walter, Nucl. Instrum. Methods Phys. Res. Sect. A Acceler. Spectrometers Detectors Assoc. Equip. 337 (1994) 486.
[27] N. Hawkes, J. Adams, D. Bond, S. Croft, O. Jarvis, N. Watkins, Nucl. Instrum. Methods Phys. Res. Sect. A Acceler. Spectrometers Detectors Assoc. Equip. 476 (2002) 190. (International Workshop on Neutron Field Spectrometry in Science, Technology and Radiation Protection).
[28] R. Brun, F. Rademakers, Nucl. Instrum. Methods Phys. Res. Sect. A Acceler. Spectrometers Detectors Assoc. Equip. 389 (1997) 81. (New Computing Techniques in Physics Research).
[29] A. Zimbal, H. Klein, M. Reginatto, H. Schuhmacher, L. Bertalot, A. Murari, High resolution neutron spectrometry with liquid scintillation detectors for fusion applications, in: Proceedings of International Workshop on Fast Neutron Detectors and Applications PoS, 2006.
[30] International Standard Organization, Reference Neutron Radiations Part I: Characteristics and Methods of Production, ISO/DIS 8529-1, 2000.
[31] C. Brient, C. Nelson, R. Young, Nucl. Instrum. Methods 98 (1972) 329.